Proceedings of Proceedings of the ASME 2021 International Technical Conference and Exhibition on Packaging and Integration of Electronic and Photonic Microsystems InterPACK2021
October 26-28, 2021, Virtual, Online

IPACK2021-69317

HOTSPOT COOLING PERFORMANCE FOR SUBMERGED CONFINED TWO-PHASE JET IMPINGEMENT COOLING

Tanvir Ahmed Chowdhury*
Graduate Research Assistant
Mechanical and Aerospace Engineering
University of Central Florida
Orlando, Florida

Shawn A. Putnam
Associate Professor
Mechanical and Aerospace Engineering
University of Central Florida
Orlando, Florida

ABSTRACT

Jet impingement can be particularly effective for removing high heat fluxes from local hotspots. Two-phase jet impingement cooling combines the advantage of both the nucleate boiling heat transfer with the single-phase sensible cooling. This study investigates two-phase submerged jet impingement cooling of local hotspots generated by a diode laser in a 100 nm thick Hafnium (Hf) thin-film on glass. The jet/nozzle diameter is ∼1.2 mm and the normal distance between the nozzle outlet and the heated surface is ∼3.2 mm. Novec 7100 is used as the coolant and the Reynolds numbers at the jet nozzle outlet range from 250 to 5000. The hotspot area is ∼ 0.06 mm^2 and the applied hotspot-to-jet heat flux ranges from 20 W/cm^2 to 220 W/cm^2. This heat flux range facilitates studies of both the single-phase and two-phase heat transport mechanisms for heat fluxes up to critical heat flux (CHF). The temporal evolution of the temperature distribution of the laser heated surface is measured using infrared (IR) thermometry. This study also investigates the nucleate boiling regime as a function of the distance between the hotspot center and the jet stagnation point. For example, when the hotspot center and the jet are co-aligned ($x/D = 0$), the CHF is found to be ∼ 177 W/cm^2 at Re ∼ 5000 with a corresponding heat transfer coefficient of ∼58 $kW/m^2.K$. While the CHF is ∼ 130 W/cm^2 at Re ∼ 5000 with a jet-to-hotspot offset of $x/D \approx 4.2$.

Keywords: Two-phase, Jet Impingement Boiling, Hotspot Cooling, Novec 7100

NOMENCLATURE

D	Diameter of the nozzle/jet, *mm*
T	Temperature, *K*
H	Distance (nozzle outlet to heated surface), *mm*
x	Lateral offset (stagnation point to hotspot center), *mm*
U	Axial jet velocity, m/s
h	Heat transfer coefficient (HTC), $kWm^{-2}K^{-1}$
q''	Applied heat flux, W/cm^2
R	Reflectivity
k	Thermal conductivity, $Wm^{-1}K^{-1}$
P	Laser power, *mW*
ONB	Onset of Nucleate Boiling, W/cm^2
CHF	Critical Heat Flux, W/cm^2
C_p	Volumetric heat capacity, $Jm^{-3}K^{-1}$

GREEK LETTERS

ν	Kinematic Viscosity, m^2/s

NON-DIMENSIONAL NUMBERS

x/D	Jet-to-Hotspot offset ratio
Re	Jet Reynolds number; $\mathrm{Re} = \mathrm{UD}/\nu$

SUBSCRIPTS or SUPERSCRIPTS

eff	Effective
Hf	Hafnium
HS	Hotspot
FS	Fused silica
f	Fluid
ROI	Region of interest
th	thermal

*Address all correspondence to this author.

INTRODUCTION

The current trend in microelectronics is to manufacture devices with increased computational powers and reduced spatial footprints. These new devices with increased power densities are consequently subject to extreme thermal loads. Thermal management of these power loads is quite challenging, especially for the next generation of 3D computing architectures where internal cooling is essential. Jet impingement is one of the top candidates for managing such extreme heat fluxes in microelectronics. Submerged and confined jet cooling configurations are popular. A submerged jet is when the cooling jet is surrounded by an environment of the same fluid. Confined jets are a type of submerged jet, where the liquid is confined between an orifice plate and the heated surface. The coolant flow-field is primarily radial. However, there are regions of high axial-to-radial flow-field curvatures, especially for confined jet impingement within a narrow gap [1]. Jet impingement cooling can produce thin, micro-scale thermal and velocity boundary layers with additional enhancements in the cooling performance via turbulent heat transfer at high Reynolds number flows [1]. In comparison to channel, flat-plate, or parallel flow cooling configurations, jet impingement can provide heat transfer coefficients (HTCs) up to three times greater.

Single-phase jet impingement performances are well documented by Zuckerman et al. [1]. Two-phase jet impingement can remove additional heat by taking advantage of the latent heat (phase-change or two-phase nucleate boiling) of the liquid at the heater wall. However, the flow-field of the impinging fluid has a complex, nonlinear coupling to both the number density and rate of vapor cavity nucleation on the heater surface. At lower heat fluxes (or wall superheats), the vapor cavities remained pinned to the heater wall. While, at increased wall superheats, these vapor cavities will detach from the hot wall heater surface. This transition is defined as the onset of nucleate boiling (ONB). This two-phase nucleate boiling regime is the ideal cooling state for removing extreme heat fluxes with relatively small wall superheats (e.g., 2-20 $^{\circ}C$). The upper-limit (or maximum) heat flux achieved in this nucleate boiling regime is well-known as the critical heat flux (CHF). Beyond CHF limit, device burnout occurs. High Reynolds number jet impingement flows in narrow gaps can increase the CHF by increasing the frequency of the nucleate boiling events at reduced wall superheats. Additionally, these boiling events can further enhance the sensible heat contributions to the cooling performance via the increased turbulent mixing of the jet's flow-field near the heater wall.

Two-phase jet impingement boiling has been studied for a few decades now. More recent studies were summarized by Qiu et al. [2]. A more focused review of submerged and confined jet impingement boiling was done by Fan et al. [3]. The effects of jet velocity and subcooling on CHF have been studied extensively. While most of the contemporary studies focus on uniformly heated surfaces, there have been some attempts at un-

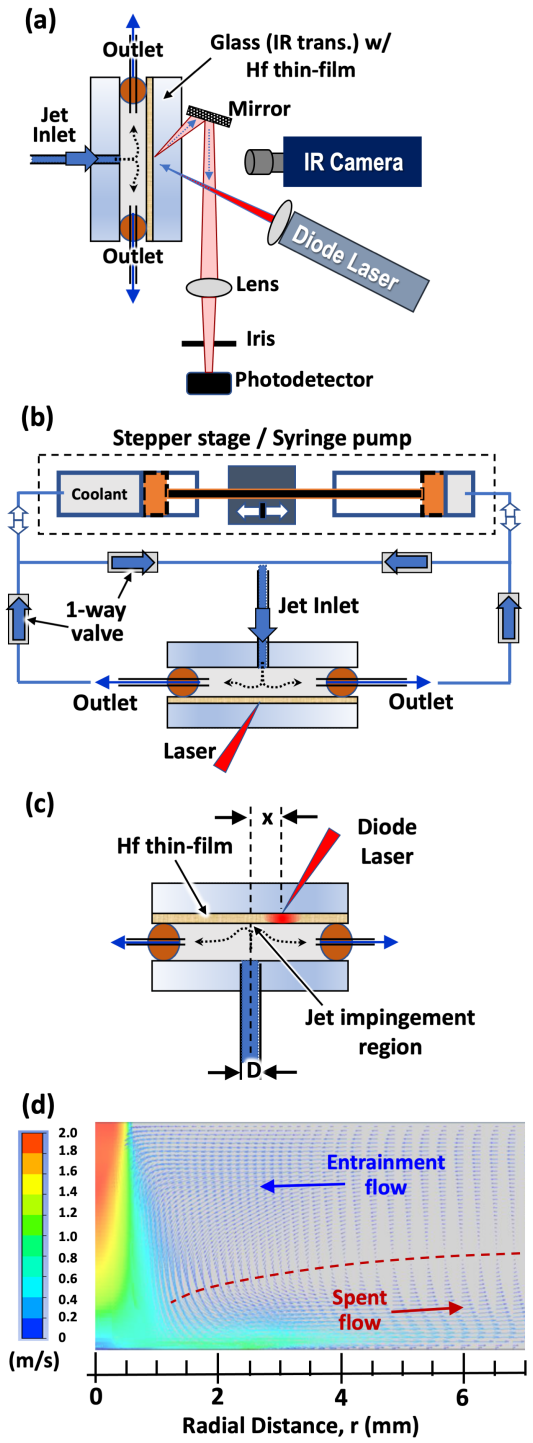

FIGURE 1. EXPERIMENTAL JET IMPINGEMENT COOLING SETUP, USING A DIODE LASER TO GENERATE A HIGH HEAT FLUX HOTSPOT AND IR THERMOMETRY TO CHARACTERIZE THE SPATIOTEMPORAL HOTSPOT TEMPERATURE.

derstanding the hotspot cooling via a single-phase jet [4] [5].

This study focuses on the localized hotspot cooling performance by two-phase jet impingement. Dielectric liquid Novec 7100, made by 3M Inc., was chosen as the jet coolant. The boiling point for Novec 7100 is 61 $^{\circ}C$. The boiling onset and the CHF are studied as a function of inlet jet velocity (or jet Reynolds number, Re). The jet Reynolds number from the nozzle outlet is varied from 250 to 5000. Additionally, this study investigates the nucleate boiling regime under the jet impingement condition with respect to jet-to-hotspot offset ratio x/D, where D is the diameter of the jet at the cooling chamber inlet and x is the lateral (radial) displacement between the jet's stagnation point and the center of the hotspot.

EXPERIMENTAL SETUP & PROCEDURE

Fig. 1 overviews the experimental setup for this work. The study is focused on jet cooling of a localized hotspot created by a diode laser. The confined jet chamber is constructed using an O-ring seal between two fused silica (FS) glass windows. One of the glass windows is coated with a thin-film of Hafnium (Hf) thin film. This Hf coating acts as both the heater and thermometer of the experimental setup. The Hf-glass window was fabricated by depositing 100 nm of Hf on an Infrared (IR) transparent FS glass window via DC magnetron sputtering. A diode laser is used to locally heat the Hf thin-film and to create the hotspot heat source, as depicted in Fig. 1a. The jet coolant is issued through the center of the glass window, such that the jet impinges on the Hf thin-film at a normal angle of incidence, as presented in Fig. 1b. Additionally, two syringe needles passing through the O-ring seal, function as the outlets for the confined jet impingement chamber. The later sections describe the hotspot heating in more detail.

Fig. 1a presents a schematic representation of the hotspot generated by heating with a focused diode laser, the cooling of the hotspot by the impinging confined jet, and the subsequent spatiotemporal temperature measurement of the Hf thin film using the IR camera. A blue laser (450 nm) is partially absorbed by the Hf thin film ($R \sim 45$ %, transmission < 0.1 %). The hotspot area in the Hf thin film is maintained to be $\sim 0.06\ mm^2$ (0.138 mm in radius) using a focusing lens. The laser power is controlled via a LED current-voltage driver. The reflected laser light from the Hf thin film is monitored by a photo-detector, where the output voltage of the photo-detector is monitored by an oscilloscope as pictorially represented in Fig. 1a. Thus, the response of the photodetector facilitates in-situ temporal heat input monitoring.

The hotspot is cooled by the jet flow-loop setup with a dual syringe pump configuration, as depicted in fig. 1b. A computer-controlled stepper stage is connected with two stainless steel piston syringes. When the stepper stage is displaced in one direction, the coolant is simultaneously displaced out of one piston syringe and into the other piston syringe. This combination of four one-way valves allows for continuous jet flow regardless of the pumping direction. The later section describes the spatiotemporal temperature evolution monitoring in more detail.

A FLIR IR camera (spectral sensitivity: 1.5 - 5 μm, pixel size $\sim 14.42\ \mu$m, window size: 160×128, and frame rate: 603 frames per second) is used to capture spatiotemporal temperature evolution of the Hf thin film. The IR camera was calibrated by using a K-type thermocouple. The accuracy of the IR camera temperature is within $\pm\ 0.2 - 0.6\ K$ when the temperature is below 40 $^{\circ}C$, whereas the uncertainty increases to $\pm\ 1 - 2\ K$ when the temperature is above 45 $^{\circ}C$. The emissivity of the Hf thin film and the transmissivity of the IR transparent FS window were measured by following the procedure outlined by FLIR [6]. Both sides of the Hf thin film are assumed to have the same temperature because the Hf film thickness is only ~ 100 nm.

To understand the cooling capability of two-phase jet impingement, when the jet stagnation point and the hotspot center are not aligned, this study varies the 'offset' between the stagnation point of the jet and the center of the hotspot. The lateral displacement between the stagnation point of the jet and the hotspot center is defined as x. This displacement is normalized by the diameter of the nozzle/jet, x/D. In this study, H/D is kept constant at a value of ≈ 2.64, where the nozzle outlet to heated surface distance is $H \approx 3.175\ mm$.

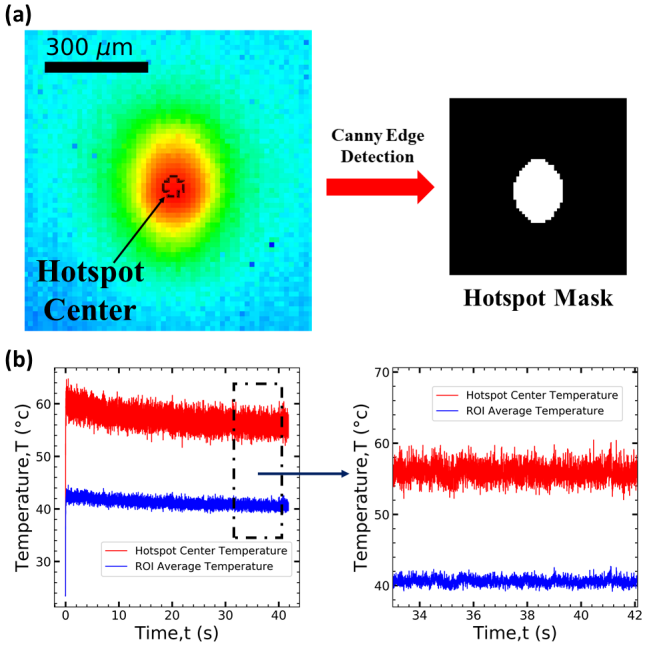

FIGURE 2. HOTSPOT MASK GENERATION FOR TRACKING BOTH THE TEMPORAL HOTSPOT CENTER TEMPERATURE AND AREA-AVERAGED (ROI/MASK) TEMPERATURE.

Since the heating condition is for a local, sub-millimeter hotspot, the captured IR images need some post-processing. Fig. 2 illustrates how the IR images captured by the IR camera are processed to extract spatiotemporal temperature information to facilitate the analysis of the experimental data. The hotspot depicted in fig. 2a corresponds to laser diode heating of a stagnant coolant pool inside the chamber (i.e., no impinging jet). Then, a combination of the Canny edge detection method [7], and the floodfill method is used to segment the hotspot region-of-interest (ROI). Afterward, this binary ROI mask is used to track the temperature within the hotspot. The binary mask is multiplied with IR images captured by the IR camera, thus, extracting the temperature information within the hotspot. Then, the area average of the hotspot temperature for each frame is calculated, which provides the temporal trend of the averaged hotspot temperature. As an example, Fig. 2b shows the temporal plot of the average temperature based on an applied hotspot-to-jet heat flux of 91.2 W/cm^2, at $Re = 5000$ and at zero jet-to-hotspot offset ratio ($x/D = 0$). Fig. 2b also presents the temporal plot of the temperature at the hotspot center for the same condition. Fig. 2b shows that when the heat flux is applied the temperature overshoots. Then, the hotspot temperature decreases gradually before becoming 'steady'. Fig. 2b also presents the time interval where the temporal temperature profile reaches a steady-state. All the results presented in this investigation corresponds to the steady-state regime for confined jet impingement cooling of a hotspot. The jet coolant temperature is within $\sim 22-23\ ^{\circ}C$, which results in $\sim 38-39\ ^{\circ}C$ subcooling.

RESULTS & DISCUSSION

Accurate predictions of the wall heat flux and heat transfer coefficient require knowledge of the conjugate heat transfer in the Hf-coated glass window. While the Hf coating is thin (e.g., 100 nm thick), there is still significant in-plane thermal conduction in this Hf coating. Based on the experimental configuration the area-averaged hotspot heat flux in the Hf thin-film heater q''_{net} can be defined as:

$$q''_{\text{net}} = \frac{P\sigma}{A_{\text{HS}}}, \tag{1}$$

where P is the laser power output, $\sigma = 1 - R$ is the amount of absorbed laser light, R is the reflectance of the Hf thin film, and A_{HS} is the hotspot area. We note that the 100 nm thick Hf thin-film is opaque at the wavelength of the diode laser. Since, this applied heat flux is being removed by the fluid, Hf thin-film, and the FS glass substrate, the relation among the applied heat flux, the heat flux removed by the fluid, and the heat flux removed by the substrate can be expressed as:

$$q''_{\text{net}} = q''_{\text{f}} + q''_{\text{FS}}, \tag{2}$$

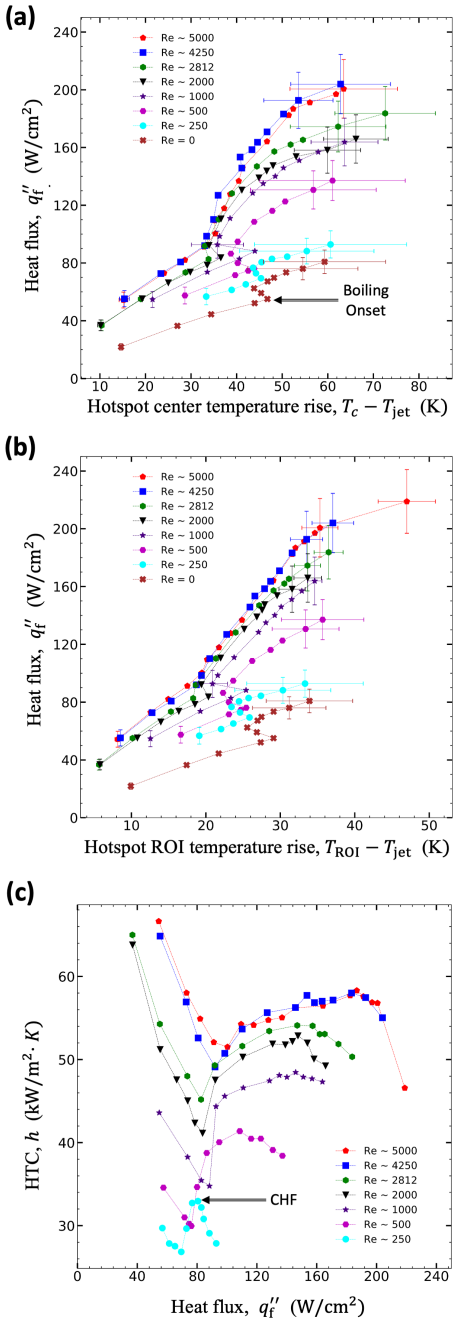

FIGURE 3. JET IMPINGEMENT COOLING PERFORMANCE FOR THE REFRIGERANT NOVEC 7100 - IN TERMS OF THE STAGNATION POINT WALL HEAT FLUX, HOTSPOT CENTER TEMPERATURE, AREA-AVERAGED HOTSPOT TEMPERATURE, THE AVEA-AVERAGED HEAT TRANSFER COEFFICIENT (HTC).

where q''_{FS} is the heat flux removed by the glass window and q''_{f} is the heat flux removed by the coolant. q''_{f} can be calculated using the following equation:

$$q''_{\mathrm{f}} = q''_{\mathrm{net}} \left(\frac{e^{\mathrm{eff}}_{\mathrm{th,f}}}{e^{\mathrm{eff}}_{\mathrm{th,f}} + e^{\mathrm{eff}}_{\mathrm{th,FS}}} \right), \tag{3}$$

where $e_{\mathrm{th,f}}$ and $e_{\mathrm{th,FS}}$ are the effective thermal effusivities of the fluid and the glass substrate, respectively. The thermal effusivities can be defined as:

$$\begin{aligned} e_{\mathrm{th,f}} &= \sqrt{k^{\mathrm{eff}}_{\mathrm{f}} C_{\mathrm{p,f}}} \\ e_{\mathrm{th,FS}} &= \sqrt{k^{\mathrm{eff}}_{\mathrm{FS}} C_{\mathrm{p,FS}}}, \end{aligned} \tag{4}$$

where $C_{\mathrm{p,f}}$ and $C_{\mathrm{p,FS}}$ are the volumetric heat capacities of the fluid and the glass substrate, respectively and $k^{\mathrm{eff}}_{\mathrm{f}}$ and $k^{\mathrm{eff}}_{\mathrm{FS}}$ are the effective thermal conductivities of the fluid and the glass substrate, respectively. The transient heat transfer from the laser-induced disc source of heat in the Hf thin-film of constant heat flux (q''_{f}) is anisotropic [8]. Therefore, the effective thermal conductivities of the fluid and glass substrates can account for the in-plane conduction in the Hf thin-film via

$$\begin{aligned} k^{\mathrm{eff}}_{\mathrm{f}} &= k^{1/3}_{\mathrm{f}} k^{2/3}_{\mathrm{Hf}} \\ k^{\mathrm{eff}}_{\mathrm{FS}} &= k^{1/3}_{\mathrm{FS}} k^{2/3}_{\mathrm{Hf}}, \end{aligned} \tag{5}$$

where k_{f}, k_{FS}, and k_{Hf} are the thermal conductivities of the fluid coolant, the glass substrate, and the Hf thin-film, respectively. We find that these expressions for the effective thermal conductivity work very well for predicting the spatiotemporal hotspot temperature for both jets and stagnant fluids (e.g., air, ethanol, etc.) with both modulated (periodic) and steady heating by the laser. For these transient heating conditions, we found that the effective thermal diffusivity is limited by the interfacial conductance (or interfacial thermal resistance) at the glass-Hf and fluid-Hf interface. For example, the effective thermal diffusivity in the FS substrate can be approximated as $\alpha^{\mathrm{eff}}_{\mathrm{th}} = \sqrt{\alpha_{\mathrm{th,FS}} \alpha_{\mathrm{th,I}}}$, where $\alpha_{\mathrm{th,I}} = G\Delta_I / C_{\mathrm{p,Hf}}$, $G \approx$150 W/m^2/K, and $\Delta_I \approx$1 nm are the corresponding interface thermal diffusivity, interfacial conductance, and interface thickness of the FS-Hf interface, respectively.

The area averaged heat transfer coefficient (h) can be expressed as:

$$h = \frac{q''_{\mathrm{f}}}{\Delta T}, \tag{6}$$

where ΔT is the difference between the coolant temperature (T_{jet}) and the time-averaged hotspot ROI-averaged temperature (T_{ROI}). As stated previously, this study presents the cooling performance of the two-phase confined jet impingement by evaluating the steady period. The steady ROI and hotspot center temperatures are time-averaged, and their standard deviations are calculated.

Fig. 3 presents the experimental heat transfer data for Re = 0, 250, 500, 1000, 2000, 2812, 4240, and 5000 as a function of heat flux at jet-to-hotspot offset ratio, $x/D = 0$. Fig. 3a and fig. 3b present the hotspot center temperature rise and the ROI averaged temperature rise at the steady time interval. For experimental data of each Reynolds number, two data points with the highest uncertainties and one data point with the lowest uncertainty are presented in fig. 3a and fig. 3b. Uncertainty in laser power output measurements, the reflectivity of the Hf surface, hotspot area, inlet jet temperature, and the fluctuations in heated surface temperature (see fig. 2b) were considered while calculating 95% confidence intervals. At lower heat flux the flow is single-phase, and the fluctuations in temperature come from the motion of the eddies present in the jet flow. At higher heat flux when the flow is two-phase, boiling events add further fluctuations in hotspot temperature. At high heat flux conditions, the hotspot center temperature fluctuations are of the order of 30 $^{\circ}C$ and the ROI average temperature fluctuation is of the order of 10 $^{\circ}C$. This high fluctuations in temperature occur due to the dry-out and subsequent wetting of the hotspot surface at heat fluxes beyond a critical heat flux. Hence, in order to avoid high temperature rise and potential device failure, the CHF needs to be mapped in terms of Reyolds number. On the other hand, fig. 3 shows that by incorporating nucleate boiling the same temperature can be maintained at a lower Reynolds number. Therefore, this study also maps the onset of nucleate boiling.

Before extracting the limits of the nucleate boiling regime, this study defines those limits to systematically compare among the experiments. At high Reynolds numbers ($Re \geq 2000$), when the hotspot center temperature reaches close to the boiling point (61 $^{\circ}C$) of the Novec 7100, the $q''/\Delta T$ increases or $\frac{\partial^2 q''}{\partial T^2}$ becomes positive. This point is defined as the onset of nucleate boiling. On the other hand, at lower Reynolds numbers (($Re \leq 1000$) the temperature rise goes beyond the boiling point before overshooting to a lower temperature, and the boiling initiates. This is defined as incipient boiling. According to Zhou et al., the liquid wetting angle is greater than the effective cone angle of the nucleation cavities, and the liquid can not fill those cavities. Once the vapor embryos obtain sufficient energy to nucleate and separate from the nucleation cavities, boiling occurs [9]. At lower Reynolds number incipient boiling is prominent. In contrast, at higher Reynolds numbers incipient boiling is suppressed. For this reason, this study uses the term 'Boiling Onset'. For lower Reynolds number this means the incipient point and for higher Reynolds number this means the onset of nucleate boiling. On the other hand, CHF is defined as the point where nucleate boiling HTC reaches local maxima or when $\partial h / \partial q'' < 0$.

The transitional heat fluxes were extracted using the previ-

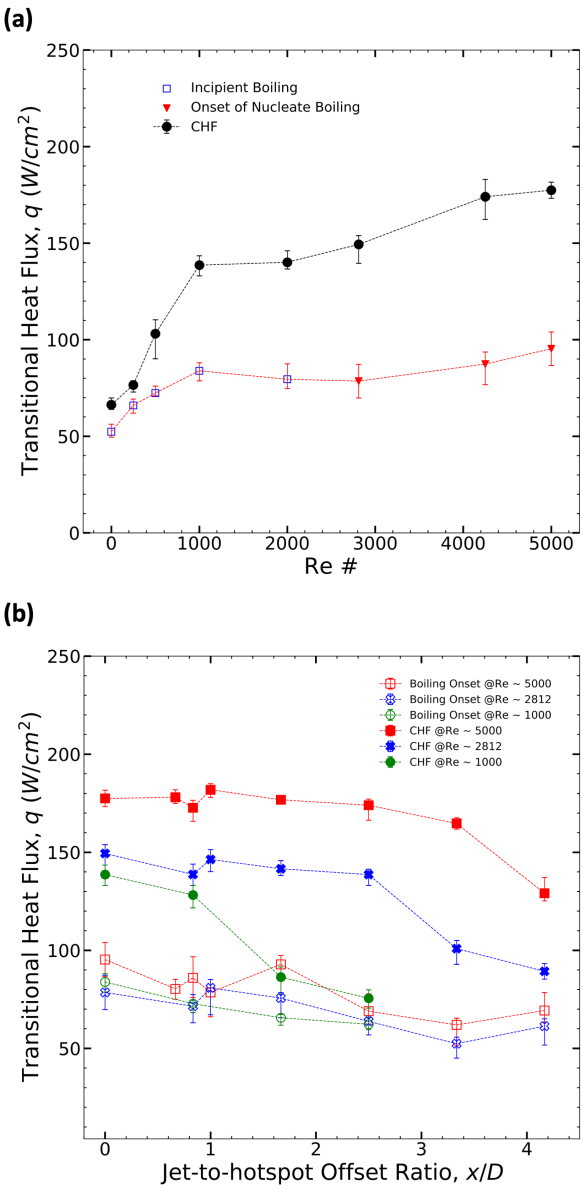

FIGURE 4. JET IMPINGEMENT COOLING PERFORMANCE WITH NOVEC 7100 IN TERMS OF THE TRANSITIONAL HEAT FLUXES MEASURED (E.G., CHF, ONB, AND INCIPIENT BOILING) AT DIFFERENT JET REYNOLDS NUMBERS AND JET-TO-HOTSPOT OFFSET RATIOS.

ously mentioned definitions and are presented with respect to Reynolds number, and jet-to-hotspot offset ratio in fig. 4. The boiling onset and the CHF are defined as the transitional heat flux. Fig. 4a presents the transitional heat flux as a function of Reynolds number, Re at jet-to-hotspot offset ratio, $x/D = 0$. Greater jet velocity/Reynolds number increases the nucleate boiling regime. The CHF and boiling onset increases sharply when the flow is laminar ($Re \leq 1000$). When the flow becomes transitional/turbulent, the rate of the transitional heat flux increment drops. Nonetheless, the CHF and the boiling onset still increase with the greater Reynolds number, and the nucleate boiling regime becomes broader.

The transitional heat fluxes are presented as a function of jet-to-hotspot offset ratio ($0 \leq x/D \leq 4.2$) for $Re = 1000$, 3000, and 5000 in fig. 4b. For laminar flow ($Re = 1000$), the CHF and the boiling onset peak at $x/D = 0$, and then the transitional heat fluxes decrease gradually. For transitional/turbulent flow ($Re =$ 3000/5000), there is another peak or a break from self-similarity at $x/D = 1$. This occurs due to the flow acceleration at the edge of the stagnation zone [10, 11]. The peak CHF for $Re = 5000$ is $\approx 180\ W/cm^2$ at $x/D \approx 1$. When $x/D > 1$, the transitional heat fluxes decrease gradually for the transitional/turbulent flow as well. The decrease rate for transitional heat flux is dependent on the Reynolds number. Local flow velocity follows a Gaussian distribution and the width of this distribution is dictated by jet entrainment [12, 13]. After the jet impinges, the spent flow can recirculate and entrain into the potential core of the incoming jet, as depicted in fig. 1d. This phenomenon increases the apparent flow rate. Due to this entrainment effect, a higher Reynolds number will provide a greater transitional heat flux limit at a high jet-to-hotspot offset ratio, and the nuclear boiling regimes will narrow at a much smaller rate with increasing x/D. This pattern shows the potential for a single submerged confined two-phase jet to effectively cool a distribution of different potential hotspot locations when $x/D \leq 4.2$ and the flow is turbulent.

CONCLUSIONS

This study investigated the cooling performance for submerged confined two-phase jet cooling local hotspot as a function of jet Reynolds number, jet-to-hotspot offset ratio, and the applied heat flux. Two-phase jet impingement proved to be capable of extending nucleate boiling regime, thus enabling high heat flux removal. It was found that the highest CHF ($\approx 180\ W/cm^2$ for $Re = 5000$ at $x/D \approx 1$) and the widest nucleate boiling regime can be expected within the stagnation zone ($x/D \leq 1$). Even at $x/D \approx 3.3$, the CHF is $\sim 166\ W/cm^2$ for $Re = 5000$. This demonstrates the capability of cooling multiple hotspot locations by the two-phase jet. Additionally, at stagnation zone ($x/D = 0$), even for a Reynolds number of 1000 the CHF is increased by roughly 100 % with respect to that of pool boiling ($Re = 0$). Additional studies with different fluids are required to develop a theoretical understanding of the impacts of varied experimental parameters and enable optimization of the pumping cost and the heat removal requirement.

ACKNOWLEDGMENT

This material is based on research sponsored by the U.S. Israel Binational Science Foundation under Grant No. 2016399. The views and conclusions contained herein are those of the authors and should not be interpreted as necessarily representing the official policies or endorsements, either expressed or implied, of the Office of the US Israel Binational Science Foundation.

REFERENCES

[1] Zuckerman, N., and Lior, N., 2006. "Jet impingement heat transfer: Physics, correlations, and numerical modeling". Vol. 39 of *Advances in Heat Transfer*. Elsevier, pp. 565 – 631.

[2] Qiu, L., Dubey, S., Choo, F. H., and Duan, F., 2015. "Recent developments of jet impingement nucleate boiling". *International Journal of Heat and Mass Transfer,* ***89***, pp. 42–58.

[3] Fan, S., and Duan, F., 2020. "A review of two-phase submerged boiling in thermal management of electronic cooling". *International Journal of Heat and Mass Transfer,* ***150***, p. 119324.

[4] Germain, T., Chowdhury, T. A., Carter, J., and Putnam, S. A., 2018. "Measuring heat transfer coefficients for microchannel jet impingement using time-domain thermoreflectance". In 2018 17th IEEE Intersociety Conference on Thermal and Thermomechanical Phenomena in Electronic Systems (ITherm), pp. 449–454.

[5] Chowdhury, T. A., Brewer, C., and Putnam, S. A., 2020. "Hotspot cooling performance of a submerged water jet via infrared thermometry". In 2020 19th IEEE Intersociety Conference on Thermal and Thermomechanical Phenomena in Electronic Systems (ITherm), pp. 166–172.

[6] Danjoux, R. Window and external optics transmittance. http://support.flir.com, 'A817-T560472_A-en-US Technical publication 60 Window or External Optics Transmittance.pdf'. Accessed: 2020-03-04.

[7] Canny, J., 1986. "A computational approach to edge detection". *IEEE Transactions on Pattern Analysis and Machine Intelligence,* ***PAMI-8***(6), Nov, pp. 679–698.

[8] Carslaw, H. S., and Jaeger, J. C., 1959. *Conduction of Heat in Solids*, 2 ed. Oxford University Press, New York, pp. 257,260,264.

[9] Zhou, D., Ma, C., and Yu, J., 2004. "Boiling hysteresis of impinging circular submerged jets with highly wetting liquids". *International Journal of Heat and Fluid Flow,* ***25***(1), pp. 81–90.

[10] Lienhard, J. H., 2006. "Heat Transfer by Impingement of Circular Free-Surface Liquid Jets". *Invited Keynote Paper, 18th National and 7th ISHMT-ASME Heat and Mass Transfer Conference*, January.

[11] Webb, B., and Ma, C.-F., 1995. "Single-phase liquid jet impingement heat transfer". Vol. 26 of *Advances in Heat Transfer*. Elsevier, pp. 105 – 217.

[12] Striegl, S. A., and Diller, T. E., 1984. "An Analysis of the Effect of Entrainment Temperature on Jet Impingement Heat Transfer". *Journal of Heat Transfer,* ***106***(4), 11, pp. 804–810.

[13] Xu, Z., Hangan, H., and Yu, P., 2008. "Analytical Solutions for a Family of Gaussian Impinging Jets". *Journal of Applied Mechanics,* ***75***(2), 02. 021019.